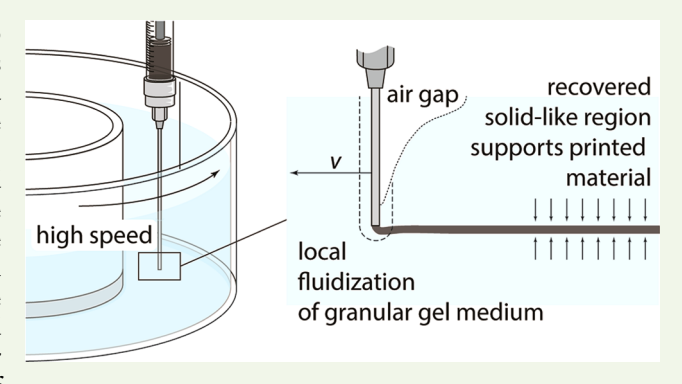


# Stability of High Speed 3D Printing in Liquid-Like Solids

Kyle J. LeBlanc,<sup>†</sup> Sean R. Niemi,<sup>†</sup> Alexander I. Bennett,<sup>†</sup> Kathryn L. Harris,<sup>‡</sup> Kyle D. Schulze,<sup>†</sup> W. Gregory Sawyer,<sup>†,‡</sup> Curtis Taylor,<sup>†</sup> and Thomas E. Angelini\*,<sup>†,§</sup>

**ABSTRACT:** Fluid instabilities limit the ability of features to hold their shape in many types of 3D printing as liquid inks solidify into written structures. By 3D printing directly into a continuum of jammed granular microgels, these instabilities are circumvented by eliminating surface tension and body forces. However, this type of 3D printing process is potentially limited by inertial instabilities if performed at high speeds where turbulence may destroy features as they are written. Here, we design and test a high-speed 3D printing experimental system to identify the instabilities that arise when an injection nozzle translates at 1 m/s. We find that the viscosity of the injected material can control the Reynold's instability, and we discover an additional, unanticipated instability near the top surface of the granular microgel medium.



KEYWORDS: 3D printing, microgel, yield stress material, liquid-like solid, high-speed, Reynold's number

In 3D printing of practically any material, fundamental technological challenges arise from the instabilities of fluids as they transition into a solid state. In advanced and wellestablished thermoplastic 3D printing systems, the precision of nozzle positioning and motion control are not the technological limitations of potential feature size, layer thickness, part reproducibility, or fidelity between a product and its design; the limits arise largely from the unstable behavior of molten plastic.<sup>1-4</sup> 3D printing with molten metal faces the same challenges; fluid instabilities compete with solidification rates even with innovative approaches that employ low-melting temperature metallic ink. 5,6 These challenges of handling and structuring fluids as they cool and solidify have also been overcome in a recent bioprinting application, in which molten sugar was 3D printed into sacrificial scaffolds that were dissolved after backfilling the open space with a biopolymer matrix.<sup>7</sup> 3D printing methods that employ gelation as a solidification strategy must also strike a delicate balance between writing rates and ink solidification rates to achieve good performance. 8-10 Many of these challenges in 3D printing are circumvented by writing into a microgel-based medium that itself transitions between solid and fluidized states under applied stress, allowing material to be placed and trapped in space without relying on the solidification of a liquid ink.<sup>11</sup> Here, instabilities arising from surface tension, gravitational sag, and interfacial wetting are eliminated. However, this material performs best when formulated to have a very low yield stress, elastic modulus, and fluidized viscosity, which introduces the possibility that printing performance will be dominated by a

totally different set of driving forces, now limited by a Reynold's instability where inertial forces overtake viscous resistance, resulting in reflow or turbulence. Considering the clear need for faster 3D printing to meet the grand challenges facing the technology, this potential instability must be investigated.<sup>12</sup>

Here, we study 3D printing into a granular microgel medium at high speeds in search of new instabilities that may limit printing performance. We introduce a simple laboratory testing system that can translate an injection nozzle through the printing medium at speeds in excess of 1 m/s (Figure 1a). At these high speeds, we are able to control a transition between controlled and unstable printing by manipulating fluid viscosity. An additional, unanticipated instability is found near the surface of the granular microgel bath, where an air gap opens up in the wake of the printing nozzle. A simple analysis of driving and viscous forces predicts the depth of this gap. The discovery of a printing speed limit that is set by Reynold's instability will provide guidance for future high speed printing research and applications.

To prepare a granular microgel medium for 3D printing, we disperse 0.2% (w/w) Carbopol ETD 2020 into ultrapure water as previously described.<sup>11</sup> These microgels are composed of lightly cross-linked poly(acrylic acid) copolymers that swell significantly, forming a jammed solid at very low polymer

Special Issue: 3D Bioprinting

Received: April 6, 2016 Accepted: August 17, 2016

<sup>&</sup>lt;sup>†</sup>Department of Mechanical and Aerospace Engineering, University of Florida, Gainesville, Florida 32611, United States

<sup>&</sup>lt;sup>‡</sup>Department of Materials Science and Engineering, University of Florida, Gainesville, Florida 32611, United States

<sup>§</sup>J. Crayton Pruitt Family Department of Biomedical Engineering, University of Florida, Gainesville, Florida 32611, United States

**ACS Biomaterials Science & Engineering** 

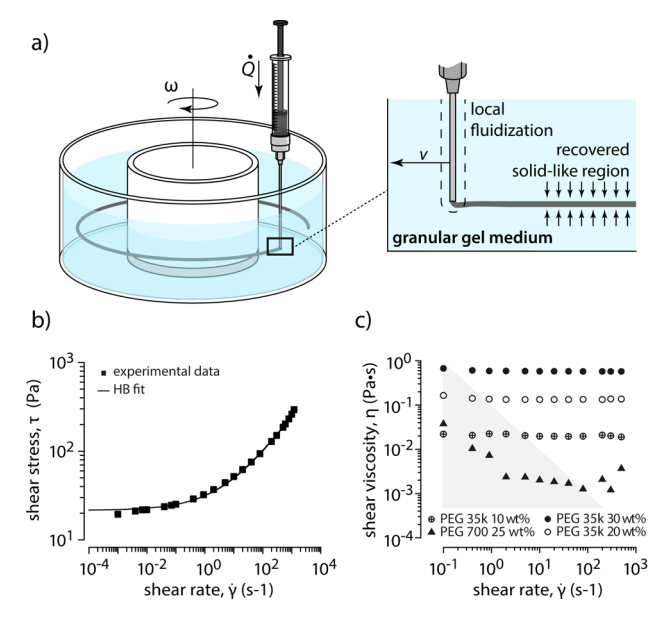


Figure 1. Schematic of testing apparatus and rheological testing data. (a) Representation of testing setup with details showing the mechanics of material deposition into the microgel. (b) Rheological testing of a microgel with Herschel-Bulkley fit showing a yield stress of  $\sim 20$  Pa. (c) Viscosity measurements for several ink materials (the shaded region is an approximate measurement of the noise floor).

concentration. Consequently, this soft, solid material has an extremely low yield stress (20 Pa) and elastic shear modulus (120 Pa), which enable it to flow under its own body forces if not supported by a container. We therefore term this material a liquid-like solid (LLS). In the experiments described here, we print features using solutions of polyethylene glycol (PEG). Fluids having a wide range of viscosities were prepared from 30%, 20%, and 10% (w/w) 35,000 molecular weight polymer and from 25% (w/w) polymer (MW 480–700), all dissolved in ultrapure water. To increase the visibility of the printed lines, colored microparticles were added to the PEG solutions.

The printing system used in these experiments is composed of three encoded linear translation stages (Newport ILS) in an XYZ configuration which provide relative motion of the injection nozzle. To achieve high translation speeds while minimizing inertial effects and vibrations of the mechanical 3D printing system itself, the X and Y motions are generated by rotating a cylindrical drum filled with LLS printing medium while translating the injection nozzle in the Z direction. We constructed an optically clear, cylindrical acrylic vessel mounted coaxially onto a hybrid stepper motor (Schneider-Electric MDrive17). Printing tests are performed at a radial distance of 83 mm from the center of rotation and at a rotational frequency of 2.01 revolutions per second, which corresponds to a relative tip speed of 1.05 m/s. A 10 mL disposable syringe with a 100 mm long stainless steel needle of outer diameter 2.1 mm is used to inject the print fluid into the LLS medium at a constant flow rate of 160  $\mu$ L/s. Displacement of the needle in the Z direction at a constant speed creates a printed helix of constant radius and pitch. All experiments were performed at an ambient temperature of 23  $\pm$  0.5 °C.

To observe the behavior of an isolated feature while printing, we perform tests in which the printing nozzle is raised rapidly, drawing a 400  $\mu$ m diameter feature into a helical shape with a 5 mm vertical pitch. When writing with the viscous, high molecular weight PEG solution, the features are observed to

be smooth and stable, exhibiting no signs of instability, despite the extremely high translation speed (Figure 2a). We quantify

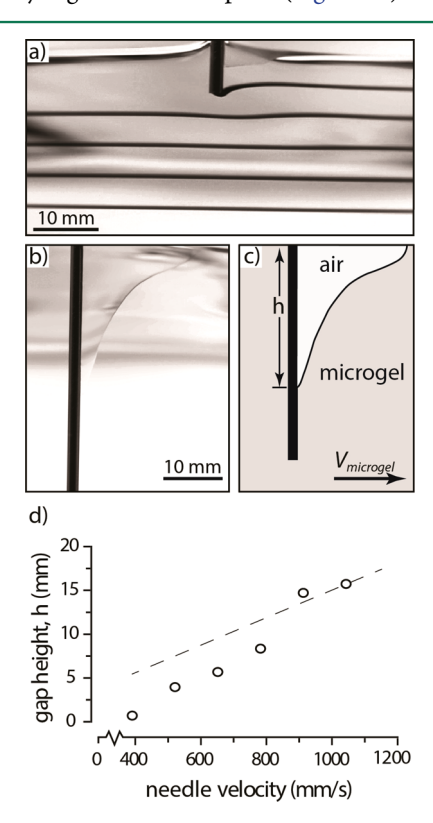


Figure 2. Images of high-speed helical printing. (a) Full field image of helix generation showing precise feature generation and deformation of support material as print "ink" is deposited. (b) Close-up of air pocket formation in needle wake. (c) Schematic of air pocket behind the needle. (d) Measurements of air gap height as a function of relative needle velocity (dashed line: approximate scaling prediction of gap height).

the feature smoothness from image analysis, finding that the standard deviation of feature thickness is 6% or about 24  $\mu$ m. To determine whether instabilities are expected under the conditions tested here, we estimate a Reynold's number, given by  $Re = \rho v d/\eta$ , where  $\rho$  and  $\eta$  are the mass density and viscosity of the PEG solution, v is the translation speed, and d is the diameter of the injection nozzle. The same form for estimating Reynold's numbers is used for numerous contexts including flow around cylinders, spheres, and inside of channels, for example. In these experiments, the shear rate can be estimated from  $\dot{\gamma} \approx v/d$ , which is approximately 500 s<sup>-1</sup>. We perform unidirectional shearing measurements with a rheometer to measure the viscosity of the PEG solution at this shear rate, which we find to be 0.6 Pa·s (Figure 1c). Combining these parameters and using the mass density of water, we find Re = 3.7. Given the smooth features written with these conditions, a midrange Reynold's number is expected, where instabilities do not dominate fluid flow.

An unanticipated phenomenon occurs at these high translation speeds; a wedge shaped crevasse filled with air opens at the top surface of the rotating LLS material in the wake of the injecting nozzle (Figure 2b,c,d). We interpret the emergence of the crevasses as an instability arising from the competition between the hydrostatic pressure that drives fluid reflow into the crevasse,  $\rho gh$ , and the viscous stress that resists this flow,  $\dot{\gamma}\eta$ . Here, h is crevasse depth, and the shear-rate,  $\dot{\gamma}$ , is the ratio of

**ACS Biomaterials Science & Engineering** 

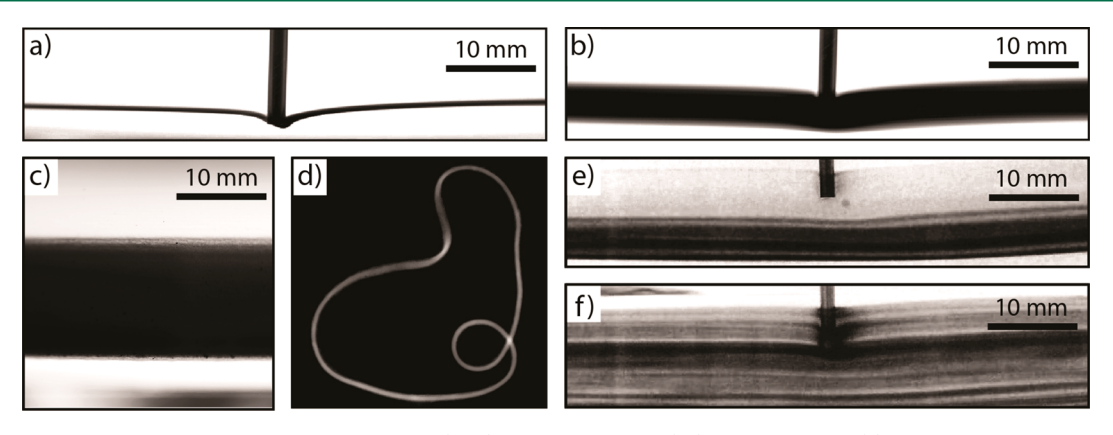


Figure 3. Images of solid band print test with high viscosity (a-d) and low viscosity (e,f) PEG solutions. (a) Image of layer-by-layer deposition in microgel during test. (b) Close-up image showing smooth layer deposition along with elastic deformation and complete recovery around the needle tip. (c) Evidence of elastic deformations are nonexistant after needle removal; no evidence of banding or lack of layer adhesion was observed. (d) 5 mm tall solid band removed from support material and swollen in a water bath. (e) PEG 20 wt % shows irregular flow around the needle tip and inconsistent deposition of material. (f) PEG 10 wt % shows increase in irregular flow and more discrete banding of the printed structure.

the crevasse refilling speed and the crevasse's width, *d*. From the filling time of 0.02 s and the crevasse depth of 16 mm, we estimate the shear rate to be 380 s<sup>-1</sup>. At this shear rate, the fluidized LLS medium has a viscosity of 1 Pa s and a corresponding shear stress of 160 Pa. Equating this stress to the hydrostatic driving pressure, we predict a crevasse depth of 16.3 mm, very close to the observed depth of 16 mm. To further test this interpretation of dynamic crevasse formation, we performed the same tests at five additional translation speeds, finding that the depth of the air gap varied proportionally with translation speed, as expected by the simple scaling model of viscous reflow (Figure 2d). Without any adjustments to the model and without adjustable fitting parameters, most data points are predicted to within less than a factor of 2.

Printing into the LLS medium at high speeds with viscous PEG ink exhibits no signs of inertial instabilities, yet the printed feature follows an upward-curved path as it exits the writing nozzle (Figure 2a). To test the origins of this curved flow field and to explore its effects on printing overlapping structures, the same tests described above were repeated with one difference; the helix, is drawn with a vertical pitch of 300  $\mu$ m per revolution, resulting in 100  $\mu$ m of overlap between successive passes (Figure 3a,b). With these tests, we find that a nearly symmetric distortion occurs on the leading side of the writing nozzle, preventing the writing nozzle from disrupting previously written layers as new layers are added, while allowing the seamless joining of successive layers (Figure 3c). It is unclear whether these effects are associated with the near-laminar flow behavior of the fluidized LLS near the writing nozzle or the elasticity of the solid regions of LLS farther from the nozzle. This effect is reminiscent of the famous demonstrations by G. I. Taylor of hydrodynamic reversibility at low Reynold's number, 13 and future work will elucidate the extent to which the two phenomena are similar.

Throughout our experimentation, questions arose about the appropriateness of applying a simple Reynold's number analysis to the granular LLS material. Since the LLS material is fluidized at the shear-rates explored here, it is treated as a high viscosity fluid ( $\eta = 270$  mPa s). To test whether the viscosity of the injected ink material dominates the fluid behavior over the fluidized LLS material, we perform a series of experiments in which PEG solutions of different viscosities are 3D printed at high speeds ( $\eta = 130$  mPa·s, 19 mPa·s, and 3.5 mPa·s). To

potentially drive these high speed 3D printing tests into the high Reynold's number regime, we once again create overlapping features under the same operating conditions as described in the previous section. For all tests with reduced viscosity and higher Reynold's numbers, the colored PEG solution collects near the tip of the nozzle in an apparent recirculating zone (Figure 3e,f), and the resulting features exhibit intermixed bands of LLS medium and PEG solution. These flow behaviors are indicative of mixing due to reflow or turbulence. 14-16 We perform the same Reynold's analysis as described above, finding Re = 17, 117, and 630, respectively, for the reduced viscosity inks. These measurements indicate that the transition into the unstable regime occurs between Re of 3.7 and 17. Theoretically, the transition into an unstable reflow regime around a cylinder occurs between Re = 10-15, 15,16 in agreement with our observations and indicating that the viscosity of the injected ink is capable of controlling the speed limit of high-speed 3D printing into LLS materials. Moreover, the potential effects of mixing the fluidized granular LLS medium with the ink appear to be small compared to the viscous shear of the ink alone. Future experiments in which the viscosity of the fluidized LLS material is varied while holding the ink-viscosity constant will help to elucidate these potential mixing effects.

In previous work, we found that polymeric precursors remain in their printed locations for many hours after deposition and could be cross-linked after printing. To verify here that the 3D printed PEG polymers do not rapidly diffuse from their deposited locations or significantly dilute during the high-speed printing process, we 3D print photo-cross-linkable solutions of PEG-diacrcrylate (MW = 480, 25% w/w) and PEG-acrylate (MW = 700, 75% w/w). After exposure to UV light and gentle agitation in a water-bath, the 3D printed structures were found to be intact and physically strong enough to be handled manually (Figure 3d). In future work, methods that directly measure the distribution of the polymeric ink should be performed in order to quantify transient effects associated with polymer diffusion or dilution before polymerization.

Here, we have shown that 3D printing in an LLS medium made from granular microgels can be performed at very high translation speeds, of the order 1 m/s. At such high speeds, the viscosity of the "inks" used in this process determines the quality of printing and stability of written features. The

properties of the granular LLS medium may become dominant at high concentrations of granular gel; permanent "cracks" may open up if the yield stress is too high and the size of the fluidized air-gap at the LLS surface may grow to unmanageable sizes if the fluidized LLS viscosity prohibits rapid reflow into the dynamic crevasse. Currently, 3D printing systems do not operate at these high speeds. However, the grand challenges in additive manufacturing like 3D organ printing require that printing speeds increase to the levels tested here and beyond. Our results indicate that when 3D printing systems achieve these high translation speeds, the limits will be set, once again, by the printing materials. A similar progression of challenges has been seen in high speed machining, where speed limits are set by the ability of metals to dissipate heat at sufficiently high rates.

#### AUTHOR INFORMATION

### **Corresponding Author**

\*E-mail: t.e.angelini@ufl.edu.

#### **Funding**

This work is funded by National Science Foundation under Grant No. DMR-1352043.

#### Notes

The authors declare no competing financial interest.

## ACKNOWLEDGMENTS

We thank Tapomoy Bhattacharjee for help with materials formulation and rheological measurements.

#### REFERENCES

- (1) Childs, T.; Berzins, M. Selective laser sintering of an amorphous polymer—simulations and experiments. *Proc. Inst. Mech. Eng., Part B* **1999**, 213 (4), 333–349.
- (2) Berzins, M.; Childs, T. H. C.; Ryder, G. R. The Selective Laser Sintering of Polycarbonate. CIRP Ann. 1996, 45 (2), 187–190.
- (3) Comb, J. W. J.; Priedeman, W. W. R.; Turley, P. W. Control Parameters and Material Selection Criteria for Fused Deposition Modeling. In *Proceedings of the Fifth International Conference on Rapid Prototyping*, University of Dayton: Dayton, OH, 1994; pp 163–170.
- (4) Yardimci, M. a; Güçeri, S. Conceptual framework for the thermal process modelling of fused deposition. *Rapid Prototyp. J.* **1996**, 2 (2), 26–31.
- (5) Wang, L.; Liu, J. Compatible hybrid 3D printing of metal and nonmetal inks for direct manufacture of end functional devices. *Sci. China: Technol. Sci.* **2014**, 57 (11), 2089–2095.
- (6) Wang, L.; Liu, J. Liquid phase 3D printing for quickly manufacturing conductive metal objects with low melting point alloy ink. Sci. China: Technol. Sci. 2014, 57 (9), 1721–1728.
- (7) Trachtenberg, J. E.; Mountziaris, P. M.; Miller, J. S.; Wettergreen, M.; Kasper, F. K.; Mikos, A. G. Open-source three-dimensional printing of biodegradable polymer scaffolds for tissue engineering. *J. Biomed. Mater. Res., Part A* **2014**, 102 (12), 4326–4335.
- (8) Yan, J.; Huang, Y.; Chrisey, D. B. Laser-assisted printing of alginate long tubes and annular constructs. *Biofabrication* **2013**, *5*, 015002.
- (9) Boland, T.; Xu, T.; Damon, B.; Cui, X. Application of inkjet printing to tissue engineering. *Biotechnol. J.* **2006**, *I* (9), 910–917.
- (10) Nishiyama, Y.; Nakamura, M.; Henmi, C.; Yamaguchi, K.; Mochizuki, S.; Nakagawa, H.; Takiura, K. Development of a three-dimensional bioprinter: construction of cell supporting structures using hydrogel and state-of-the-art inkjet technology. *J. Biomech. Eng.* **2009**, *131* (3), 035001.
- (11) Bhattacharjee, T.; Zehnder, S. M.; Rowe, K. G.; Jain, S.; Nixon, R. M.; Sawyer, W. G.; Angelini, T. E. Writing in the granular gel medium. *Sci. Adv.* **2015**, *1* (8), e1500655.

- (12) Miller, J. S. The Billion Cell Construct: Will Three-Dimensional Printing Get Us There? *PLoS Biol.* **2014**, *12* (6), e1001882.
- (13) Taylor, G. I. Film Notes for Low Reynolds-Number Flows; National Comittee for Fluid Mechanics Films: Cambridge, MA, 1967. (14) Thom, A. The Flow Past Circular Cylinders at Low Speeds.
- Proc. R. Soc. London, Ser. A 1933, 141 (845), 651–669.
  (15) Taneda, S. Experimental Investigation of the Wakes behind Cylinders and Plates at Low Reynolds Numbers. J. Phys. Soc. Jpn. 1956,
- 11 (3), 302–307.
- (16) Coutanceau, M.; Defaye, J.-R. Circular Cylinder Wake Configurations: A Flow Visualization Survey. *Appl. Mech. Rev.* **1991**, 44 (6), 255.